

# Journal of Materials Chemistry C

Accepted Manuscript



This is an *Accepted Manuscript*, which has been through the Royal Society of Chemistry peer review process and has been accepted for publication.

*Accepted Manuscripts* are published online shortly after acceptance, before technical editing, formatting and proof reading. Using this free service, authors can make their results available to the community, in citable form, before we publish the edited article. We will replace this *Accepted Manuscript* with the edited and formatted *Advance Article* as soon as it is available.

You can find more information about *Accepted Manuscripts* in the [Information for Authors](#).

Please note that technical editing may introduce minor changes to the text and/or graphics, which may alter content. The journal's standard [Terms & Conditions](#) and the [Ethical guidelines](#) still apply. In no event shall the Royal Society of Chemistry be held responsible for any errors or omissions in this *Accepted Manuscript* or any consequences arising from the use of any information it contains.

## ARTICLE

# Heavy Doping of S<sub>2</sub> in Cu<sub>7.2</sub>S<sub>4</sub> Lattice into Chemically Homogeneous Superlattice Cu<sub>7.2</sub>S<sub>x</sub> Nanowires: Strong Photoelectric Response

Cite this: DOI: 10.1039/x0xx00000x

Y. H. Gao,<sup>a,\*</sup> P. P. Wang,<sup>b</sup> M. H. Zhang,<sup>a</sup> Y. Lei,<sup>a</sup> H. L. Niu,<sup>c</sup> P. J. Li,<sup>a</sup> W. J. Fa<sup>a</sup> and Z. Zheng<sup>a,\*</sup>Received 00th January 2012,  
Accepted 00th January 2012

DOI: 10.1039/x0xx00000x

www.rsc.org/

This is the first time a series of chemically homogeneous superlattice Cu<sub>7.2</sub>S<sub>x</sub> ( $x = 4.07, 4.52, 6.01, 6.20, 6.45$ ) nanowires have been successfully synthesized by heavy doping of S<sub>2</sub> species in Cu<sub>7.2</sub>S<sub>4</sub> lattice through a simple wet-chemical route. The present superlattice structure is a polytypoid structure tuned by adjusting the atom ratio of S<sub>2</sub> to S in lattice configuration. The perfect superlattice Cu<sub>7.2</sub>S<sub>6.20</sub> structure interestingly consists of two alternating lattice fringes corresponding to the atom layers of Cu–S and Cu–S<sub>2</sub> in the even spacing of 5.70 Å. The article describes the formation, morphology, composition and structure of the Cu<sub>7.2</sub>S<sub>x</sub> superlattice nanowires. Photoluminescence (PL) spectra and transient photovoltage (TPV) measurements reveal that the generation and separation efficiency of photogenerated charges of Cu<sub>7.2</sub>S<sub>x</sub> nanowires could be improved greatly by adjusting the S<sub>2</sub>/S ratio in lattice configuration and thus enhance the luminescence quantum efficiency. This study reveals that the S<sub>2</sub> species in Cu<sub>7.2</sub>S<sub>x</sub> nanowires plays a very important role in determining the dynamic properties of photogenerated charge carriers.

## Introduction

Semiconductor superlattice nanowires with periodic composition modulations are considered as ordered heterostructures, which often exhibits unique photoelectric, thermoelectric and superconducting properties.<sup>[1,2]</sup> By changing thickness and compositional elements in each layer, it is often possible to optimize the desired properties of the system. Superlattice nanowires have been successfully prepared layer-by-layer using vacuum deposition techniques *via* altering the reaction atmosphere periodically. For example, Lieber et al.<sup>[2b]</sup> synthesized GaAs–GaP segments on the same superlattice nanowire using laser ablation of GaAs and GaP solids. Fei and co-workers synthesized Bi/Sb superlattice nanowire with a clear interface between Bi and Sb segment by means of a pulsed electrodeposition technique.<sup>[4]</sup> Recently, Zou and co-workers synthesized superlattice CdS/CdS:SnS<sub>2</sub> microwires with ordered CdS and SnS<sub>2</sub> nanosized heterostructures by a improved coevaporation technique.<sup>[5]</sup> Zn-doped In<sub>2</sub>O<sub>3</sub>–SnO<sub>2</sub> superlattices with nanosized heterostructures were prepared layer-by-layer *via* the thermal chemical vapor transport and condensation using Au as a catalyst.<sup>[6]</sup> Particularly, there are some effort on short-period superlattice heterostructures, such as InAlO<sub>3</sub>(ZnO)<sub>m</sub> ( $m=10,15$ ) nanowires,<sup>[7]</sup> In<sub>2-x</sub>Ga<sub>x</sub>O<sub>3</sub>(ZnO)<sub>3</sub> nanobelts,<sup>[8]</sup> Sn-doped In<sub>2</sub>O<sub>3</sub>(ZnO)<sub>m</sub> ( $m=4,5$ ) nanowires,<sup>[9]</sup> InGaO<sub>3</sub>(ZnO)<sub>m</sub> ( $m=3,5$ ) nanowires,<sup>[10]</sup> and Ga-doped

In<sub>2</sub>O<sub>3</sub>(ZnO)<sub>3</sub> nanobelts.<sup>[11]</sup> However, it is difficult to achieve superlattice structure in the shortest period of as alternate layer by the above layer-by-layer deposition techniques.<sup>[12]</sup> Until now, the shortest period superlattice type is still highly desired because of its exciton confinement in two alternately interleaved atom layers to modulate electrons and photons.

In this work, we report a novel and convenient chemical synthesis of S<sub>2</sub><sup>2-</sup>-doped Cu<sub>7.2</sub>S<sub>x</sub> superlattice nanowires, by reacting Cu(NO<sub>3</sub>)<sub>2</sub> and sulfur powders in NaOH aqueous solution. The uniqueness in this reaction design is the use of alkaline sulfur aqueous solution of NaOH. It is well known that NaOH is very efficient for sulfur activation into active polysulfide ions (S<sub>n</sub><sup>2-</sup>,  $n>8$ ), and further generate S<sub>2</sub><sup>2-</sup> and additional species, such as S<sub>2</sub><sup>2-</sup> and S<sub>3</sub><sup>2-</sup>. Using homologous S<sub>2</sub><sup>2-</sup> in appropriate amounts to substitute for the bridging sulfur (S<sup>2-</sup>) in Cu<sub>7.2</sub>S<sub>4</sub> units allows us to fabricate the S<sub>2</sub><sup>2-</sup>-doped Cu<sub>7.2</sub>S<sub>x</sub> ( $x = 4.07, 4.52, 6.01, 6.20, 6.45$ ) superlattice nanowires. It is found that the perfect Cu<sub>7.2</sub>S<sub>6.20</sub> superlattice structure interestingly consists of two alternating lattice fringes corresponding to the atom layers of Cu–S and Cu–S<sub>2</sub> in the even spacing of 5.70 Å. The article describes the formation, morphology, composition and structure of the Cu<sub>7.2</sub>S<sub>x</sub> superlattice nanowires. Photoluminescence (PL) spectra and transient photovoltage (TPV) measurements reveal that the presence of S<sub>2</sub> species in Cu<sub>7.2</sub>S<sub>x</sub> nanowires plays a very important role in determining their luminescence quantum efficiency and the dynamic properties of photogenerated charge carriers.

## Experimental

### Materials and methods

All reagents were of analytical grade and were used without further purification. To start the synthesis, NaOH (0.1 mol), distilled water (25 mL) and appropriate amounts of S powder (1.5, 3.0, 4.5, 6.0, 7.5 mmol, respectively) were put in a 100 mL flask with heating and stirring at 90 °C for 3h to make an alkaline sulfur aqueous solution. Different amounts of S were used to control compositions of the resulting nanowires. Then 1.5 mL of Cu(NO<sub>3</sub>)<sub>2</sub> aqueous solution (0.5 M) was injected into the alkaline sulfur aqueous solution. The resulting S<sub>2</sub><sup>2-</sup>-doped Cu<sub>7.2</sub>S<sub>x</sub> nanowires were obtained after drying the solution in vacuum oven at 180 °C for 1 h, and then annealed at 180 °C for an additional 8 h. The nanowires were collected and washed with distilled water for several times, and then dried under vacuum.

### Measurements

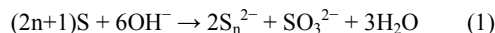
X-ray diffraction (XRD) patterns were recorded with a Philips MPD 18801 diffractometer using Cu-K $\alpha$  radiation ( $\lambda = 1.54178 \text{ \AA}$ ). Scanning electron microscopy (SEM) micrographs were taken using a JSM-5600 scanning electron microscope coupled with energy dispersive X-ray spectroscopy (EDS). The high resolution TEM (HRTEM) images and the select-area electron diffraction (SAED) patterns were obtained with a JEOL JEM 2100 high-resolution transmission electron microscope operated at 200 kV. The Raman spectrum was recorded using a LABRAM-1B confocal laser micro-Raman spectrometer with the wavelength of 632.8 nm. Ultraviolet visible (UV-vis) absorption spectra were obtained using a Shimadzu UV-3600 UV-Vis-NIR spectrophotometer. Photoluminescence (PL) spectra were obtained at room temperature using a Hitachi F-4500 fluorescence spectrophotometer. The room temperature luminescence quantum efficiency (QE) of sample was measured in ethanol with the excitation wavelength of 370 nm (3.35 eV), by using quinine sulfate in 1N sulfuric acid as a reference, whose quantum efficiency (QE) have been well-known as 0.55 in the literature.<sup>[13]</sup> The quantum efficiency (QE) of sample was finally decided by comparing the integrated emission of sample to that of quinine sulfate at an identical optical density of 0.1–0.12. The transient photovoltage (TPV) responses were determined by a homemade measurement system.<sup>[14]</sup> A parallel-plate capacitor-like sample chamber consisted of the BiVO<sub>4</sub> electrode, a piece of 10  $\mu\text{m}$  thick mica and a platinum wire gauze electrode. The samples were excited with a laser radiation pulse (wavelength of 355 nm and pulse width of 5 ns) from a Polaris II third-harmonic Nd/YAG laser. The TPV signal was registered by a 500 MHz TDS 5054 digital phosphor oscilloscope.

## Results and discussion

### Preparation of the alkaline sulfur aqueous solution

At this stage, an appropriate amount of S powders (1.5, 3.0, 4.5, 6.0, 7.5 mmol, respectively) were dissolved in an aqueous solution of NaOH (4M, 25mL) at 90 °C for 3h. While the solution color changed from yellow to orange to red within 1h, then to pale yellow

color for 2h overtime, and no S precipitation was observed in the final pale yellow alkaline sulfur aqueous solution. The color change was reminiscent of the formation of polysulfide ions (S<sub>n</sub><sup>2-</sup>, n>8) in the well-known reaction between S and NaOH aqueous solution (Eq. (1)).



With increasing n, the S<sub>n</sub><sup>2-</sup> solution colour turns from yellow to orange and then to red. We believe the existence of polysulfide ions (S<sub>n</sub><sup>2-</sup>) with long S chains makes the red polysulfide precursors more reactive than its yellow and orange counterparts, as the S–S bond in long sulfur chain is much weaker and active due to electron delocalization along the whole S<sub>n</sub><sup>2-</sup> chain. Thus, the red polysulfide precursors (S<sub>n</sub><sup>2-</sup>) are sufficiently active to generate S<sup>2-</sup> and additional species, such as S<sub>2</sub><sup>2-</sup> and S<sub>3</sub><sup>2-</sup> (Eq. (2)), resulting in the final pale yellow colour.

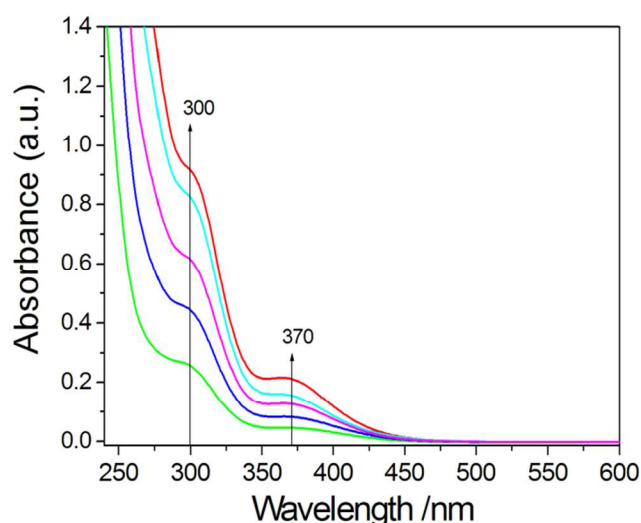
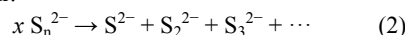


**Figure 1.** Changes in UV-Vis absorption spectra of the final pale yellow alkaline sulfur aqueous solution diluted 50 times with distilled water. The content of sulfur in reactants is 1.5, 3.0, 4.5, 6.0, 7.5 mmol, respectively.

The final pale yellow alkaline sulfur aqueous solution was monitored by a UV-vis spectrophotometer. As shown in **Figure 1**, high absorbance is observed in the 250–280 nm regions, confirming that large amounts of S<sup>2-</sup> species were produced. The absorption band at 300 nm is mainly derived from S<sub>2</sub><sup>2-</sup>, while the absorption band at 370 nm is attributed to S<sub>3</sub><sup>2-</sup>. This assignment of spectral bands is consistent with previous reports, in which sulfur was electrochemically reduced in *N,N'*-Dimethylformamide<sup>[15]</sup> or chemically reduced with alkali metals such as Li, Na, K, or Cs in tetrahydrofuran.<sup>[16]</sup> From the UV-vis absorption behavior displayed in this experiment, an increase in reactant sulfur content leads to increased absorbance at all three wavelengths; considerable amounts of S<sup>2-</sup> and more S<sub>2</sub><sup>2-</sup> and S<sub>3</sub><sup>2-</sup> species are produced with higher concentrations of sulfur in the alkaline aqueous solution. No other S<sub>n</sub><sup>2-</sup> species are produced in the present reaction condition, such as S<sub>4</sub><sup>2-</sup> (absorption at 420 nm), S<sub>5</sub><sup>2-</sup> (absorption at 438 nm), and S<sub>6</sub><sup>2-</sup> (absorption at 450 nm), etc. In this experiment, the different amounts of powdered sulfur were used to control the ratio of S<sub>2</sub><sup>2-</sup> in the alkaline sulfur aqueous solution, and further tune the composition

and structure of the resulting  $S_2^{2-}$ -doped  $Cu_{7.2}S_x$  nanowires (as listed in Table 1).

### Preparation of $Cu_{7.2}S_x$ nanowires

The resulting  $S_2^{2-}$ -doped  $Cu_{7.2}S_4$  nanowires were obtained by adding  $Cu(NO_3)_2$  aqueous solution (0.5 M, 1.5 mL) into the pale yellow alkaline sulfur aqueous solution above, then drying the solution in a vacuum oven at 180 °C for 1 h and then annealing at 180 °C for an additional 8 h. In fact, to obtain the

target products, the molar ratio of powdered sulfur to  $Cu(NO_3)_2$  must be in the range of 2–10 equivalents. Controlling the molar ratio of S and  $Cu(NO_3)_2$  for 2:1, the  $Cu_{7.2}S_{4.07}$  samples were prepared. When the sulfur content was increased further to be in the range of 4–10 equiv, the other  $Cu_{7.2}S_x$  series ( $x=4.52, 6.01, 6.20$  and  $6.45$ ) were obtained (Table 1). The Cu/S atomic ratio in the  $Cu_{7.2}S_x$  series was validated with energy-dispersive X-ray spectroscopy (EDS) (Figure S1).

**Table 1.** Compositions and lattice parameters of  $Cu_{7.2}S_x$  nanowires prepared with reactants of various S/  $Cu(NO_3)_2$  molar ratios.

Content of sulphur in reactants	S/ $Cu(NO_3)_2$ molar ratios in reactants	Compositions of $Cu_{7.2}S_x$ nanowires		$Cu_{7.2}S_x$	Lattice parameter $a$
		Cu/S atomic percentages	Cu/S atomic ratios		
1.5 mmol	2:1	63.89 : 36.11	7.2 : 4.07	$Cu_{7.2}S_{4.07}$	5.5590 Å
3.0 mmol	4:1	61.45 : 38.55	7.2 : 4.52	$Cu_{7.2}S_{4.52}$	5.5499 Å
4.5 mmol	6:1	54.49 : 45.51	7.2 : 6.01	$Cu_{7.2}S_{6.01}$	5.5341 Å
6.0 mmol	8:1	53.70 : 46.30	7.2 : 6.20	$Cu_{7.2}S_{6.20}$	5.5171 Å
7.5 mmol	10:1	52.76 : 47.24	7.2 : 6.45	$Cu_{7.2}S_{6.45}$	5.4940 Å

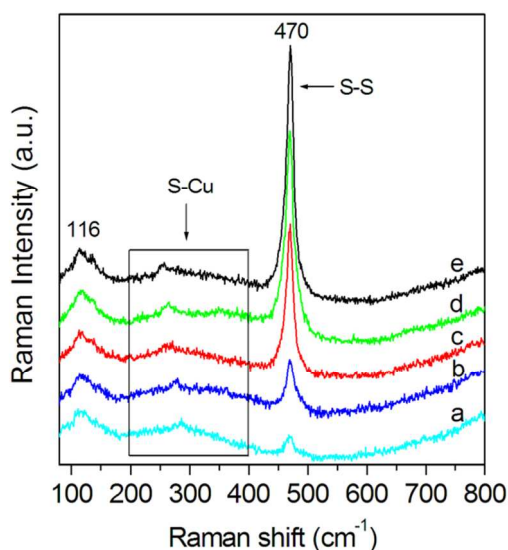


**Figure 2.** Raman spectrum of the  $S_2^{2-}$ -doped  $Cu_{7.2}S_x$  samples of a)  $Cu_{7.2}S_{4.07}$ ; b)  $Cu_{7.2}S_{4.52}$ ; c)  $Cu_{7.2}S_{6.01}$ ; d)  $Cu_{7.2}S_{6.20}$ ; e)  $Cu_{7.2}S_{6.45}$ .

The increasing S atomic ratio is due to more  $S_2^{2-}$  species replacing the  $S^{2-}$  in  $Cu_{7.2}S_x$  unit, which was validated by Raman investigation. While the  $S_3^{2-}$  species can't be combined into  $Cu_{7.2}S_x$  lattice at 180 °C due to its steric bulkiness or decomposition to  $S^{2-}$  and  $S_2^{2-}$ . As shown in Figure 2, the Raman spectrum of all the obtained samples exhibit three distinct vibrational signals: S–S vibrational mode at 470  $cm^{-1}$ ,<sup>[17]</sup> Cu–S vibrational mode in a broad range of 400  $cm^{-1}$  to 200  $cm^{-1}$ ,<sup>[18]</sup> and the surface optical phonon mode at 116  $cm^{-1}$ .<sup>[19]</sup> In the  $Cu_{7.2}S_{4.07}$  sample, the weaker S–S stretching signal at 470  $cm^{-1}$  indicates there were only a few sulfur dimers ( $S_2^{2-}$ ) in the  $Cu_{7.2}S_{4.07}$  lattice, since the S–S vibration mode typically produces a strong Raman signal.<sup>[17]</sup> For the other  $Cu_{7.2}S_x$  samples, the S–S stretching signal at 470  $cm^{-1}$  shows a characteristic and systematic intensity increase with the

increasing S atomic ratio, indicating the introduction of more sulfur dimers ( $S_2^{2-}$ ) in the lattice. The peak resulting from the Cu–S vibration mode is typically reported at 335  $cm^{-1}$ .<sup>[18]</sup> However, the corresponding peak in our spectra is obviously shifted in energy and exhibits a broad range from 400  $cm^{-1}$  to 200  $cm^{-1}$ . We propose that the broad Cu–S vibration mode could be the result of anion exchange between  $S^{2-}$  and  $S_2^{2-}$ , which would generate additional stretching signals corresponding to the Cu–S and Cu– $S_2$  vibration modes. Also, the broad Cu–S vibration signal would offer the possibilities that there may be some degree of strong electronic effects of  $S_2^{2-}$  with respect to their neighboring copper atoms, improving the bond strength and force constant in the whole lattice.

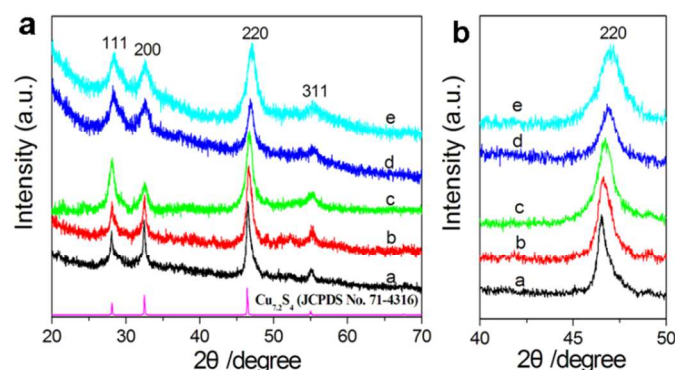


**Figure 3.** a) XRD patterns of the as-prepared  $S_2^{2-}$ -doped  $Cu_{7.2}S_x$  samples, and b) an expanded view of the (220) peaks. Patterns of a)  $Cu_{7.2}S_{4.07}$ ; b)  $Cu_{7.2}S_{4.52}$ ; c)  $Cu_{7.2}S_{6.01}$ ; d)  $Cu_{7.2}S_{6.20}$ ; e)  $Cu_{7.2}S_{6.45}$ .

Figure 3a shows XRD data of the as-prepared  $Cu_{7.2}S_x$  ( $x=4.07, 4.52, 6.01, 6.20$  and  $6.45$ ) samples. These diffraction patterns are consistent with the features of the digenite  $Cu_{7.2}S_4$  in face-centered cubic phase (JCPDS No. 71-4316). All of the diffraction peaks can be readily indexed to the (111), (200), (220) and (311) planes based on the face-centered cubic  $Cu_{7.2}S_4$ . Nevertheless, the diffraction angles of the peaks in the patterns are significant bigger than that of

$\text{Cu}_{7.2}\text{S}_4$ , implying a lattice contraction of the  $\text{Cu}_{7.2}\text{S}_x$  series. **Figure 3b** shows an expanded view of the (220) diffraction peak of the  $\text{Cu}_{7.2}\text{S}_x$  series. With the S atomic ratio varying from 4.07 to 6.45, the diffraction peak of the (220) crystal plane shifts from  $46.14^\circ$  to  $46.72^\circ$ , and the calculated cell constant  $a$  decreases from  $5.5590 \text{ \AA}$  to  $5.4940 \text{ \AA}$  (**Table 1**), which is much smaller than that of  $\text{Cu}_{7.2}\text{S}_4$  ( $a = 5.57 \text{ \AA}$ ). The difference could not be explained by a measurement error of the XRD equipment, which is less than  $0.005 \text{ \AA}$ . Also, the successive diffraction peak shifts indicated that the obtained  $\text{S}_2^{2-}$ -doped  $\text{Cu}_{7.2}\text{S}_x$  nanocrystals were in a solid solution similar to that of the reported  $\text{Cu}_{2-x}(\text{S}_y\text{Se}_{1-y})$  solid solution,<sup>[20]</sup> ruling out the possibility of phase separation or separated nucleation of nanocrystals. Considering the stronger electronic effects of  $\text{S}_2^{2-}$  than  $\text{S}^{2-}$  due to the orbital hybridization and electron delocalization in the sulfur dimer ( $\text{S}_2^{2-}$ ), it is reasonable to expect that  $\text{S}_2$  species occupy the sites of S atom in the lattice; this results in increased bond strength and force constant, and thus leads to the significant decrease in the lattice constant  $a$ . This explanation is consistent with the Raman results above.

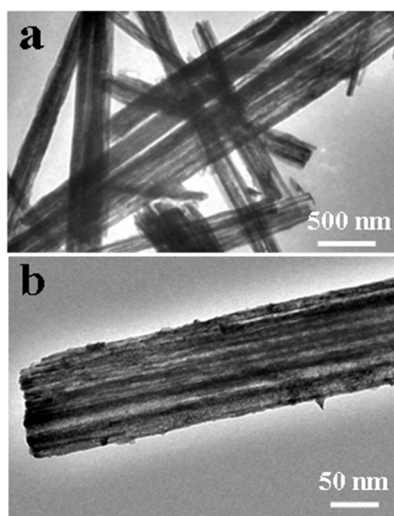


**Figure 4.** TEM images of the  $\text{Cu}_{7.2}\text{S}_{6.20}$  nanowires: a) A low-magnification image of the  $\text{Cu}_{7.2}\text{S}_{6.20}$  nanowires; b) an individual nanowire shows surface schistous structure along its entire length.

The samples' morphology was studied by TEM. **Figure 4a** shows a low-magnification image of the  $\text{Cu}_{7.2}\text{S}_{6.20}$  samples. It appears that each of the wire-like structures is an aggregate of many smaller nanowires of about  $100\text{--}150 \text{ nm}$  in diameter. To better observe the morphologies, an individual nanowire is shown in **Figure 4b**. Its surface appears to have a schistous structure along the entire length. For all of the  $\text{S}_2^{2-}$ -doped  $\text{Cu}_{7.2}\text{S}_x$  series, their morphologies show negligible differences.

#### Superlattice structural properties of $\text{Cu}_{7.2}\text{S}_x$ nanowires

To obtain more detailed structural information on the  $\text{S}_2^{2-}$ -doped  $\text{Cu}_{7.2}\text{S}_x$  series, high-resolution TEM (HRTEM) and select-area electron diffraction (SAED) measurements were performed. For the  $\text{Cu}_{7.2}\text{S}_{4.07}$  nanowire, the SAED pattern, as shown in inset in **Figure 5a**, gives a set of diffraction spots corresponding to the face-centered cubic structure, in which the

spot indexed as spot (220) relates to a plane distance of  $1.95 \text{ \AA}$ , while spot (111) and spot (11 $\bar{1}$ ) correspond to  $3.28 \text{ \AA}$  and  $3.26 \text{ \AA}$ , respectively. All these values are slight aberration from the values of the face-centered cubic  $\text{Cu}_{7.2}\text{S}_4$ .

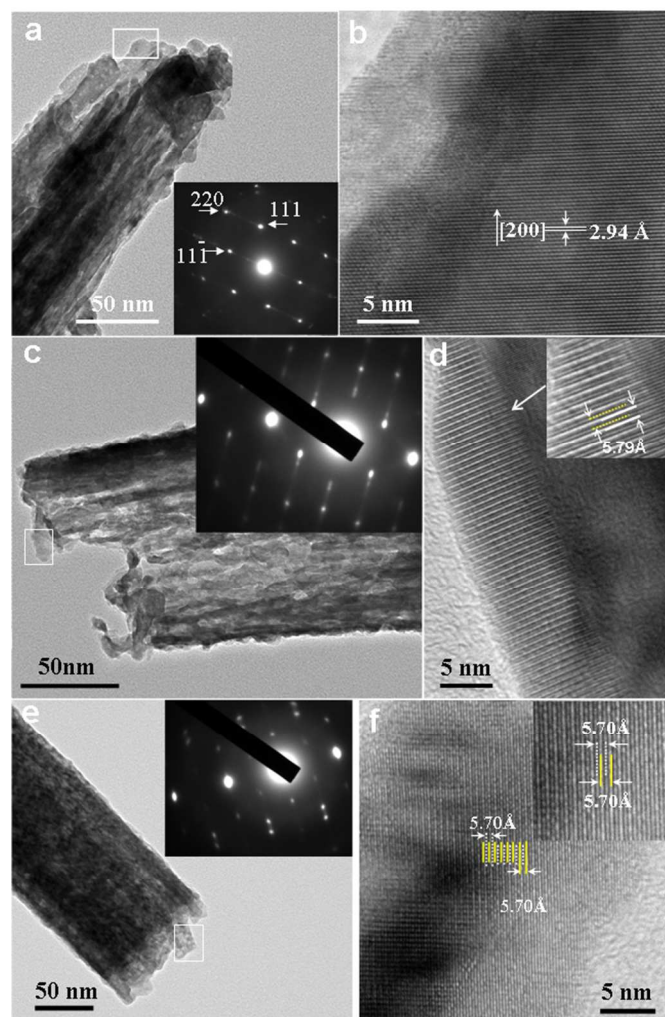


**Figure 5.** TEM images and HRTEM images of a,b)  $\text{Cu}_{7.2}\text{S}_{4.07}$  nanowire; c,d)  $\text{Cu}_{7.2}\text{S}_{6.01}$  nanowire; e,f)  $\text{Cu}_{7.2}\text{S}_{6.20}$  nanowire. Inset in TEM image is the corresponding SAED pattern of the nanowire.

Interestingly, the diffraction spots are in an almost continuous line between two main diffraction spots, which is indeed a characteristic of superlattice structure.<sup>[3,7,10,11]</sup> Also, the observed lattice spacing of  $2.94 \text{ \AA}$  (**Figure 5b**), indexed to the (200) plane, is larger than that in a normal face-centered cubic  $\text{Cu}_{7.2}\text{S}_4$  structure, which is  $2.79 \text{ \AA}$ . However, due to few  $\text{S}_2$  species in the  $\text{Cu}_{7.2}\text{S}_{4.07}$  nanowire, the superlattice structure is too obscure to observe (**Figure 5b**). With the heavy doping of  $\text{S}_2$  species, such as  $\text{Cu}_{7.2}\text{S}_{6.01}$  nanowires, the superlattice characteristic obviously appear. The characteristic subcell spots of the SAED of the superlattice structure indicate a good commensurability (**Inset in Figure 5c**). As shown in **Figure 5d**, the HRTEM image of the area marked in **Figure 5c** clearly reveals a novel superlattice structure. It is very clear that the image consists of lattice fringes periodically interleaved by

alternately bright and dark contrast lines. There are only two different lattice fringes alternately interleaved in the same spacing about 5.79 Å as an alternate layer. The distance between two adjacent lattice fringes is about 2.89 Å corresponding to the (200) plane, which is smaller than that (2.94 Å) in  $\text{Cu}_{7.2}\text{S}_{4.07}$  structure. Note that, among all of the  $\text{S}_2^{2-}$ -doped  $\text{Cu}_{7.2}\text{S}_x$  samples, the  $\text{Cu}_{7.2}\text{S}_{6.20}$  nanowires exhibited the perfect superlattice structure. A series of clear subcell diffraction spots in the SAED pattern (Inset in Figure 5e) indicate the perfect commensurability in the  $\text{Cu}_{7.2}\text{S}_{6.20}$  superlattice structure. As shown in Figure 5f, the perfect periodical superlattice structure spans the whole area marked in Figure 5e. It is very clear that the superlattice structure has a short period of two atom layers alternately interleaved by smooth and wavy lattice fringes with even 5.70 Å spacing. Also, the distance between the two adjacent lattice fringes is 2.85 Å, smaller than that (2.89 Å) in the  $\text{Cu}_{7.2}\text{S}_{6.01}$  superlattice structure. This is the first time such a modulation structure has been observed in superlattice structures. Typically, the commensurability of superlattice structure is the result of dopants that diffuse throughout the whole lattice and form modulated structures corresponding to a stable atom arrangement in the lattice configuration.<sup>[10]</sup> We believe that the present superlattice structure is a polytypoid structure tuned by adjusting the ratio of  $\text{S}_2$  to S species in lattice. Particularly, with increasing  $\text{S}_2$  species, the adjacent fringe spacing successive decrease, so the alternately lattice fringes may correspond to the Cu–S layer and Cu– $\text{S}_2$  layer, respectively. For the perfect  $\text{Cu}_{7.2}\text{S}_{6.20}$  superlattice structure, there should be roughly half of the S atoms have been substituted by  $\text{S}_2$  species. It is worth noting that the composition of  $\text{Cu}_{7.2}\text{S}_{6.20}$  can be represented formally as  $\text{Cu}_{7.2}(\text{S})_2(\text{S}_2)_{2.1}$ . This may cause more even alternative stacking of Cu–S layer and Cu– $\text{S}_2$  layer to form the periodic modulated structure.

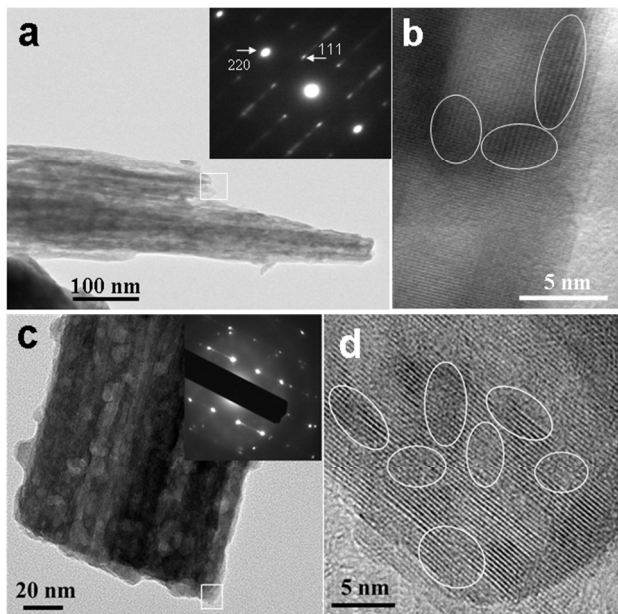


**Figure 6.** TEM images and HRTEM images of a,b)  $\text{Cu}_{7.2}\text{S}_{4.52}$  nanowire; c,d)  $\text{Cu}_{7.2}\text{S}_{6.45}$  nanowire. Inset in TEM image is the corresponding SAED pattern of the nanowire.

From these results, it can be concluded that the  $\text{S}_2$  species in appropriate amounts with an even atom arrangement in whole lattice should be essential for the good commensurability of the superlattice structure. In fact, for  $\text{Cu}_{7.2}\text{S}_{4.52}$  nanowires, due to less  $\text{S}_2$  species atoms in the lattice configuration, the superlattice characteristic is only reflected in the SAED pattern, and the corresponding HRTEM image shows the regionally located modulated structures with imperfect commensurability (Figure 6a,b). Conversely, for  $\text{Cu}_{7.2}\text{S}_{6.45}$  nanowires, the commensurability of superlattice structure is also destroyed due to more dopant atoms in disorder in the lattice configuration. As shown in inset in Figure 6c, the diffraction spots imply an incompetent commensurability. Also, the lattice image in Figure 6d shows many crystal defects such as vacancies, where an atom is missing altogether, and dislocations, where the perfection of the structure is disrupted along a line.

#### Photoelectric properties of $\text{Cu}_{7.2}\text{S}_x$ nanowires

In order to investigate the photoelectric properties of  $\text{Cu}_{7.2}\text{S}_x$  nanowires, we acquired photoluminescence (PL) spectra of those  $\text{Cu}_{7.2}\text{S}_x$  nanowires at room temperature.

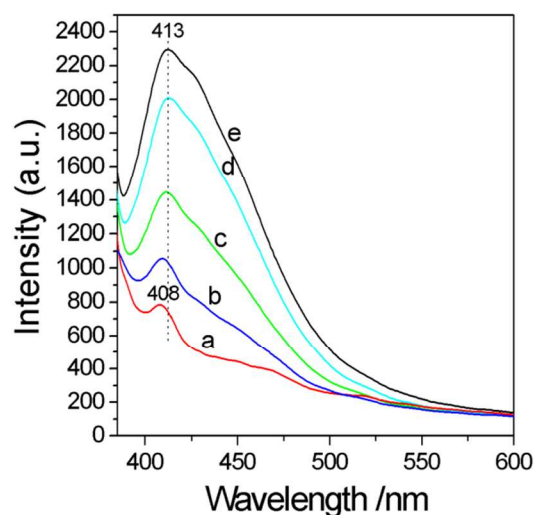


**Figure 7.** Photoluminescence (PL) spectra of the  $\text{Cu}_{7.2}\text{S}_{4.07}$  (a),  $\text{Cu}_{7.2}\text{S}_{4.52}$  (b),  $\text{Cu}_{7.2}\text{S}_{6.01}$  (c),  $\text{Cu}_{7.2}\text{S}_{6.20}$  (d) and  $\text{Cu}_{7.2}\text{S}_{6.45}$  nanowires (e) with excitation wavelength at 325 nm

As shown in Figure 7a, the PL spectra of  $\text{Cu}_{7.2}\text{S}_{4.07}$  nanowires have a weak emission band peaking at 408 nm, attributed to near band edge (NBE) emission due to the recombination of the free excitons. Furthermore, a broad emission shoulder emerges in the visible region of 425–550 nm. Interestingly, with the  $x$  value varying from 4.07 to 6.45 in  $\text{Cu}_{7.2}\text{S}_x$  nanowires, the dominant NBE emission band seriously broadens with a stronger emission shoulder extending to 550 nm (Figure 7b). Moreover, the NBE emission peak red-shifts to lower energy (413 nm). From the five PL spectra, we could identify comparable trends in the integrated luminous intensity, which is significantly stronger with increasing  $\text{S}_2$  species. The luminescence quantum efficiency (QE) is about 9% for the  $\text{Cu}_{7.2}\text{S}_{4.07}$  nanowires, 55% for  $\text{Cu}_{7.2}\text{S}_{6.20}$  nanowires, and 59% for  $\text{Cu}_{7.2}\text{S}_{6.45}$  nanowires, respectively. In our cases, the increasing

NBE emission and stronger emission shoulder must be related to the doping of  $S_2$  species in  $Cu_{7.2}S_4$  lattice, which improve the dynamic properties of photoinduced charge carriers.

The transient photovoltage (TPV) spectroscopy technique was used to further investigate the dynamic properties of photoinduced charge carriers in those  $S_2^{2-}$ -doped  $Cu_{7.2}S_x$  samples. It can provide direct information about the charge dynamics, including the generation, separation, and recombination of photoinduced charge carriers.<sup>[21]</sup>

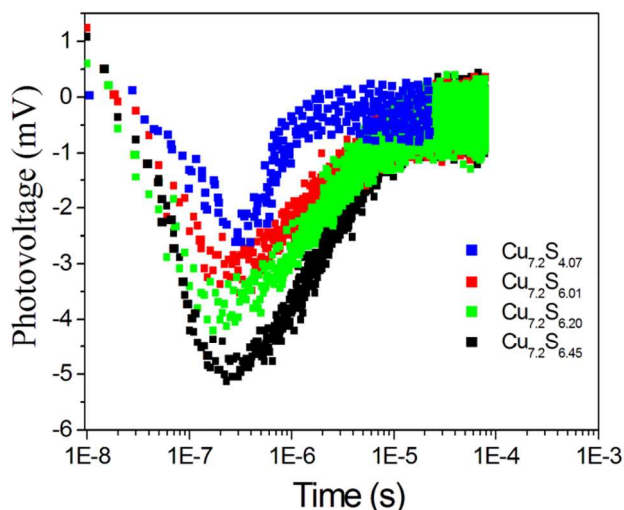


**Figure 8.** Transient photovoltage spectroscopy (TPS) of  $Cu_{7.2}S_{4.07}$  nanowires,  $Cu_{7.2}S_{6.01}$ ,  $Cu_{7.2}S_{6.20}$  and  $Cu_{7.2}S_{6.45}$  nanowires excited by a 355 nm laser pulse.

Figure 8 shows the TPV responses of  $Cu_{7.2}S_{4.07}$ ,  $Cu_{7.2}S_{6.01}$ ,  $Cu_{7.2}S_{6.20}$  and  $Cu_{7.2}S_{6.45}$  nanowires excited by a 355 nm laser pulse. The  $Cu_{7.2}S_{4.07}$  nanowires displayed a negative photovoltage transient signal with an abrupt rise to TPV maximum ( $t_{max}$ ) at  $2 \times 10^{-7}$  s. Afterward, the TPV signal is sharply weakened with response times of  $2 \times 10^{-7}$ – $2 \times 10^{-6}$  s as a result of recombination processes of the photogenerated charges. The short lifetime suggests a low separation efficiency of the photogenerated charges in  $Cu_{7.2}S_{4.07}$  nanowires. In general, the negative TPV response means photoinduced electrons accumulate at the top electrode under irradiation, which indicates that a built-in electric field dominates the charge separation.<sup>[22]</sup> We believe that a few of  $S_2$  species in the  $Cu_{7.2}S_{4.07}$  compound could result in a compositional gradient of  $S/S_2$  in  $Cu_{7.2}S_{4.07}$  nanowires. The compositional gradient of  $S/S_2$  and the nature of copper-poor compounds induce the presence of internal electric field in  $Cu_{7.2}S_{4.07}$  nanowires. As a result, the photogenerated electrons could move to the surface of  $Cu_{7.2}S_{4.07}$  nanowires induced by the self-built electric field. Thus, a negative signal of the TPV response at  $2 \times 10^{-7}$  s for  $Cu_{7.2}S_{4.07}$  nanowires is the result of photogenerated electrons drift under the self-built electric field at the surface region. Similarly to the  $Cu_{7.2}S_{4.07}$  nanowires, the heavy doping of  $S_2$  species in  $Cu_{7.2}S_x$  samples could lead to uneven compositional gradient of  $S/S_2$  in nanocrystallites, which is expected to facilitate the efficient charge separation and transfer. As shown in **Figure 8**, the three samples of  $Cu_{7.2}S_{6.01}$ ,  $Cu_{7.2}S_{6.20}$  and  $Cu_{7.2}S_{6.45}$  nanowires all

have a strong TPV response in negative signal with response times of  $1 \times 10^{-7}$  s under the irradiation of 355 nm laser. It can be observed that the TPV response intensity was obviously strengthened with the increasing  $S_2$  species in those  $Cu_{7.2}S_x$  samples, implying the generation of photoinduced charge carriers in more high concentrations. More significantly, the lifetime of the excess charge carriers for the three samples became much longer ( $1 \times 10^{-7}$ – $2 \times 10^{-5}$  s) than that of  $Cu_{7.2}S_{4.07}$  ( $2 \times 10^{-7}$ – $2 \times 10^{-6}$  s), indicating that the improved separation of photoinduced electron–hole pairs was achieved by the heavy doping of  $S_2$  species. This result gives us an indirect evidence for the existence of effective self-built electric field in those  $Cu_{7.2}S_x$  nanowires, which can efficiently increase the generation and separation efficiency of the photogenerated charge carriers. However, the detail properties of the self-built electric field are not yet clear and still need to be further studied.

## Conclusions

In conclusion, a series of  $S_2^{2-}$ -doped  $Cu_{7.2}S_x$  ( $x = 4.07, 4.52, 6.01, 6.20, 6.45$ ) nanowires with tunable polytypoid structures have been successfully synthesized by a simple wet-chemical route at an annealing temperature of 180 °C. The presence of  $S_2^{2-}$  facilitates the formation of homologous  $Cu_{7.2}S_x$  superlattice structures, which is different from heterogeneous and chemically nonhomogeneous superlattice nanowires. The  $Cu_{7.2}S_x$  superlattice structures display the shortest period ever observed of two atom layers, consisting of Cu–S and Cu– $S_2$ . The as-obtained  $Cu_{7.2}S_x$  superlattice nanowires exhibit an intense emission with luminescence quantum efficiency (QE) of about 55%–59%, due to the heavy doping of  $S_2$  species in lattice configuration. TPV measurements demonstrate that the presence of  $S_2$  species and the nature of copper-poor compounds could induce a built-in electric field in the  $Cu_{7.2}S_x$  nanowires, which increase efficiently the generation and separation efficiency of the photogenerated charge carriers and thus improve their photoluminescence properties. This new wet-chemical method for  $Cu_{7.2}S_x$  superlattice nanowires is indeed a successful self-doping process, which could be applied to other homologous compounds with novel superlattice structures and desirable photoelectric properties.

## Acknowledgements

This work was supported by the National Natural Science Foundation of China (21271152, 21273192, 51102204, 21007053), Innovation Scientists and Technicians Troop Construction Projects of Henan Province (Grant No. 144200510014), and the Program for Science & Technology Innovation Talents in Universities of Henan Province (2011HASTIT029).

## Notes and references

<sup>a</sup> Key Laboratory of Micro-Nano Materials for Energy Storage and Conversion of Henan Province and Institute of Surface Micro and Nano Materials, Xuchang University, Henan 461000, China.

E-mail: gyh-2007@sohu.com; zhengzhi99999@gmail.com

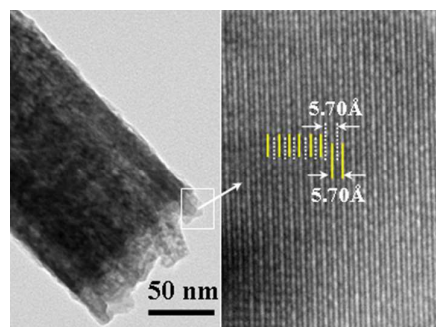
<sup>b</sup> College of Chemistry and Molecular Engineering, Zhengzhou University, Zhengzhou 450000, China.

<sup>c</sup> Department of Chemistry, Anhui University, Hefei 230039, China.

Electronic Supplementary Information (ESI) available: EDS spectra for Cu<sub>7</sub>2S<sub>x</sub> nanowires. See DOI: 10.1039/b000000x/

- 1 a) X. Duan, Y. Huang, R. Agarwal, C. M. Lieber, *Nature*, 2003, **421**, 241; b) X. D. Wang, J. H. Song, J. Liu, Z. L. Wang, *Science*, 2007, **316**, 102; c) A. I. Boukai, Y. Bunimovich, J. Tahir-Kheli, J. K. Yu, W. A. Goddard, J. R. Heath, *Nature*, 2008, **451**, 168; d) T. Burgess, S. Breuer, P. Caroff, J. Wong-Leung, Q. Gao, H. H. Tan, C. Jagadish, *ACS Nano*, 2013, **7**, 8105; e) M. Martín-González, G. J. Snyder, A. L. Prieto, R. Gronsky, T. Sands, A. M. Stacy, *Nano Lett.*, 2003, **3**, 973; f) Y. K. Liu, J. A. Zapien, Y. Y. Shan, C. Y. Geng, C. S. Lee, S. T. Lee, *Adv. Mater.*, 2005, **17**, 1372; g) C. S. Jung, H. S. Kim, H. S. Im, Y. S. Seo, K. Park, S. H. Back, Y. J. Cho, C. H. Kim, J. Park, J. P. Ahn, *Nano Lett.*, 2013, **13**, 543.
- 2 a) C. M. Lieber, *Nano Lett.*, 2002, **2**, 81; b) X. F. Zhai, C. S. Mohapatra, A. B. Shah, J. M. Zuo, J. N. Eckstein, *Adv. Mater.*, 2010, **22**, 1136; c) J. M. Aneta, J. Romaneh, U. S. Gamini, P. Z. Francis, *Small*, 2007, **3**, 722; d) F. Boxberg, N. Søndergaard, H. Q. Xu, *Adv. Mater.*, 2012, **24**, 4692; e) D. Li, Y. J. Wu, R. Fan, P. D. Yang, A. Majumdar, *Appl. Phys. Lett.*, 2003, **83**, 3186; f) D. W. Kim, I. S. Hwang, S. J. Kwon, H. Y. Kang, K. S. Park, Y. J. Choi, K. J. Choi, J. G. Park, *Nano Lett.*, 2007, **7**, 3041; g) M. S. Gudiksen, L. J. Lauhon, J. F. Wang, D. C. Smith, C. M. Lieber, *Nature*, 2002, **415**, 617; h) A. Vomiero, M. Ferroni, E. Comini, G. Faglia, G. Sberveglieri, *Nano Lett.*, 2007, **7**, 3553.
- 3 X. T. Zhang, H. Q. Lu, H. Gao, X. J. Wang, H. Y. Xu, Q. Li, S. K. Hark, *Cryst. Growth Des.*, 2009, **9**, 364.
- 4 F. H. Xue, G. T. Fei, B. Wu, P. Cui, L. D. Zhang, *J. Am. Chem. Soc.*, 2005, **127**, 15348.
- 5 G. Z. Dai, B. S. Zou, Z. L. Wang, *J. Am. Chem. Soc.*, 2010, **132**, 12174.
- 6 N. W. Wang, Y. H. Yang, J. Chen, N. S. Xu, G. W. Yang, *J. Phys. Chem. C*, 2010, **114**, 2909.
- 7 D. L. Huang, L. L. Wu, X. T. Zhang, *J. Phys. Chem. C*, 2010, **114**, 11783.
- 8 L. L. Wu, F. W. Liu, Z. Q. Chu, Y. Liang, H. Y. Xu, H. Q. Lu, X. T. Zhang, Q. A. Li, S. K. Hark, *CrystEngComm*, 2010, **12**, 2047.
- 9 C. W. Na, S. Y. Bae, J. H. Park, *J. Phys. Chem. B*, 2005, **109**, 12785.
- 10 D. P. Li, G. Z. Wang, Q. H. Yang, X. Xie, *J. Phys. Chem. C*, 2009, **113**, 21512.
- 11 L. L. Wu, Q. Li, X. T. Zhang, T. Y. Zhai, Y. Bando, D. Golberg, *J. Phys. Chem. C*, 2011, **115**, 24564.
- 12 a) R. S. Wagner, W. C. Ellis, *Appl. Phys. Lett.*, 1964, **4**, 89; b) T. E. Clark, P. Nimmatoori, K. K. Lew, L. Pan, J. M. Redwing, E. C. Dickey, *Nano Lett.*, 2008, **4**, 1246.
- 13 a) J. N. Dernas, G. A. Crosby, *J. Phys. Chem.*, 1971, **75**, 991; b) C. Querner, P. Reiss, J. Bleuse, A. Pron, *J. Am. Chem. Soc.*, 2004, **126**, 11574.
- 14 S. Pang, T. F. Xie, Y. Zhang, X. Wei, M. Yang, D. J. Wang, Z. Du, *J. Phys. Chem. C* 2007, **111**, 18417.
- 15 D. H. Han, B. S. Kim, S. J. Choi, Y. J. Jung, J. Kwak, S. M. Park, *J. Electrochem Soc.*, 2004, **151**, E283.
- 16 S. I. Tobishima, H. Yamamoto, M. Matsuda, *Electrochim. Acta*, 1997, **42**, 1019.
- 17 R. Laitinen, R. Steudel, *J. Mol. Struct.*, 1980, **68**, 19.
- 18 a) Y. J. Xiao, H. Q. Cao, K. Y. Liu, S. C. Zhang, V. Chernov, *Nanotechnology*, 2010, **21**, 145601; b) C. H. Chung, S. H. Li, B. Lei, W. B. Yang, W. W. Hou, B. Bob, Y. Yang, *Chem. Mater.*, 2011, **23**, 964.
- 19 C. R. Andrew, H. Yeom, J. S. Valentine, B. G. Karlsson, N. Bonander, G. Pouderoyen, G. W. Canters, T. M. Loehr, J. S. Loehr, *J. Am. Chem. Soc.*, 1994, **116**, 11489.
- 20 J. Xu, Y. B. Tang, X. Chen, C. Y. Luan, W. F. Zhang, J. A. Zapien, W. J. Zhang, H. L. Kwong, X. M. Meng, S. T. Lee, C. S. Lee, *Adv. Funct. Mater.*, 2010, **20**, 4190.
- 21 a) X. Y. Li, Y. Hou, Q. D. Zhao, G. H. Chen, *Langmuir*, 2011, **27**, 3113; b) P. Wang, T. F. Xie, H. Y. Li, L. L. Peng, Y. Zhang, T. S. Wu, S. Pang, Y. F. Zhao, D. J. Wang, *Chem.-Eur. J.*, 2009, **15**, 4366; c) L. L. Peng, T. F. Xie, Y. C. Lu, H. M. Fan, D. J. Wang, *Phys. Chem. Chem. Phys.*, 2010, **12**, 8033.
- 22 a) J. Jiang, X. Zhang, P. B. Sun, L. Z. Zhang, *J. Phys. Chem. C*, 2011, **115**, 20555; b) H. M. Fan, T. F. Jiang, H. Y. Li, D. J. Wang, L. L. Wang, J. L. Zhai, D. Q. He, P. Wang, T. F. Xie, *J. Phys. Chem. C*, 2012, **116**, 2425; c) J. L. Zhai, L. L. Wang, D. J. Wang, H. Y. Li, Y. Zhang, D. Q. He, T. F. Xie, *ACS Appl. Mater. Interfaces*, 2011, **3**, 2253.

Graphical Abstract:



Chemically homogeneous superlattice  $\text{Cu}_{7.2}\text{S}_x$  nanowires are constructed by heavy doping of  $\text{S}_2$  species in  $\text{Cu}_{7.2}\text{S}_4$  lattice.